IEEE Access
Multidisciplinary ⋮ Rapid Review ⋮ Open Access Journal

Received 20 November 2022, accepted 9 December 2022, date of publication 31 January 2023, date of current version 22 May 2023.

Digital Object Identifier 10.1109/ACCESS.2023.3240957

RESEARCH ARTICLE

The Domain Decomposition Method With Adaptive Time Step for the Transient Thermal Analysis of 3-D ICs

NA LIU[1], (Member, IEEE), CHENYANG WANG[1], XI CHEN[1], QIUYUE WU[1], QIQIANG LIU[1], MINGWEI ZHUANG[1], (Member, IEEE), LINLIN SHI[2], AND QING HUO LIU[3], (Fellow, IEEE)

[1]Fujian Provincial Key Laboratory of Electromagnetic Wave Science and Detection Technology, Institute of Electromagnetics and Acoustics, Xiamen University, Xiamen 361005, China
[2]Fifth Electronics Research Institute of Ministry of Industry and Information Technology, Guangzhou 511370, China
[3]Department of Electrical and Computer Engineering, Duke University, Durham, NC 27708, USA

Corresponding authors: Mingwei Zhuang (mw.zhuang@xmu.edu.cn) and Linlin Shi (shilinlin@ceprei.com)

This work was supported in part by the National Natural Science Foundation of China under Grant 61871340, and in part by the Opening Project of Science and Technology on Reliability Physics and Application Technology of Electronic Component Laboratory under Grant ZHD202107-008(135).

ABSTRACT With the continuous emergence of various advanced packaging technologies such as copper interconnection and 3-D packaging technology, it is essential to efficiently and accurately investigate the thermal analysis of high-performance, high-power and complicated electronic devices to better design heat dissipation structures. However, multiscale transient thermal analysis of complex electronic devices by existing numerical methods is still a challenge. In this work, the 3-D domain decomposition method (DDM) with the adaptive time step for the transient thermal analysis of integrated circuits (ICs) is proposed to tackle this problem. By flexible multiscale mesh generation and automatically time step changes based on posteriori errors, the new method significantly improves computational efficiency. Some illustrative numerical examples are presented to verify the accuracy and efficiency of the proposed method by considering 3-D transient heat transfer with thermal conduction, natural convection and radiation boundaries.

INDEX TERMS Thermal analysis, integrated circuits (ICs), domain decomposition method (DDM), adaptive time step.

I. INTRODUCTION

As system-level packaging technology gradually matures, the number of transistors on a single chip has reached several billion, and their feature sizes are continuously declining [1]. Meanwhile, through-silicon via (TSV)-the advanced 3-D integrated chip technology is utilized to further enhance the vertical integration of the same processes or distinct processes chips [2], [3], [4]. The resulting interconnect density and compactness achievable by TSV technology exceed what is currently possible by other packaging methods. Consequently, the heating rate per unit area of the chips is increasing, which severely challenges thermal reliability and service life of electronic equipment [5], [6].

The associate editor coordinating the review of this manuscript and approving it for publication was Su Yan.

In order to better implement thermal analysis on complex integrated circuits (ICs), several numerical methods have been proposed since the 1990s [7], such as the boundary element method (BEM) [8], the finite difference method (FDM) [9], [10], and the finite element method (FEM) [11], [12]. Among them, FEM is widely employed in terms of its versatility to conform to complex geometries and model heterogeneous materials. More accurate results can be obtained by utilizing higher-order basis functions as well as finer meshes [13], [14]. However, besides the complexity, the sizes of 3-D IC components differ by several orders of magnitude, conformal mesh in FEM will lead to enormous elements and a great increase in degrees of freedom (DoFs). Fortunately, the domain decomposition method (DDM) is proposed to handle the multiscale problems [15], [16], [17], [18]. It is applicable to divide the whole IC structure into non-overlapping

This work is licensed under a Creative Commons Attribution 4.0 License. For more information, see https://creativecommons.org/licenses/by/4.0/

subdomains according to the scales of its different parts, which would facilitate the decrease of the DoFs in the whole numerical computation.

Recently, interests have focused on the field of ICs thermal simulation by DDM. Different from the traditional FEM, DDM can naturally decompose the original multiscale problems into several easily implemented small-scale subdomains. The matrix equations are locally established with their dimensions equalling the number of DoFs of each non-overlapping subdomains [19]. Consequently, the inversion or factorization of system matrices can greatly alleviate the computational burden. However, to make DDM work for multiple subdomains, proper numerical fluxes are usually required at interfaces between the adjacent subdomains to conserve the continuity of the temperature field and normal continuity of the heat flux [20]. There are two main types of DDM according to different numerical fluxes: Lagrange multiplier-based DDM (LM-DDM) and interior penalty-based DDM (IP-DDM). LM-DDM which is represented by the finite element tearing and interconnecting (FETI) has been proposed where the enforcement of the continuity condition is realized by introducing Lagrange multipliers [21], [22]. Compared to the LM-DDM, no Lagrange multipliers is needed in IP-DDM. Instead, the Robin-transmission condition (TC) is enforced by IP weak formulation to guarantee continuities across the subdomain interfaces. Different IP-DDM algorithms also have been proposed and obtained great effectiveness for multiscale models [16], [23], [24], [25].

For temporal discretization, several numerical methods have been used for the transient thermal analysis of 3-D ICs [26], [27]. Among them, the typical explicit time methods include: forward Euler method [19] and leapfrog method [23]. The implicit time discretization methods are backward Euler method [16], [18], [22], [25] and Laguerre polynomials method [21]. DDM can be well combined with these time-domain algorithms. For example, in [19], an element-level DDM with the forward Euler method is employed to analyze the heat transfers in 3-D integrated circuits and packages with multiscale geometries. [25] utilizes non-conformal mesh with the backward Euler method to analyze the 3-D chip-package-PCB models, compared with the explicit solution method, the implicit method consumes more computation in each incremental step. Nevertheless, it generates an unconditionally stable system which is irrespective of time interval. Besides the forward and backward Euler time stepping schemes, adaptive time step is becoming a popular method [28], [29], [30], by setting the Adams-Bashforth formula as the prediction term and the trapezoidal formula as the difference between correction terms, the adaptive method has been successfully employed in computational fluid [31]. Out of the need for efficiently and accurately numerical modeling, the adaptive time scheme based on FEM has been applied to microwave heating [32] and thermal analysis of 3-D ICs [33].

In this work, incorporating adaptive time step, the DDM technique is employed to generate a good-quality finite element mesh and reduce the unknowns for 3-D complex ICs. By combining the advantages of DDM and adaptive time step, the new method can not only flexibly obtain mesh generation but also automatically control time step. Compared with the existing works, the DDM with adaptive time step is proposed for the first time to analyze the transient heat transfer of 3-D ICs. The proposed method has fewer DoFs and faster time iteration through domain decomposition and adaptively regulating time steps. The numerical performances of some typical 3-D IC structures are thoroughly investigated in this work to verify the accuracy and efficiency of the proposed new method. The rest of this paper is organized as follows: Section II describes the theoretical and mathematical details of the proposed DDM algorithm with adaptive step time discretization, as well as the establishment of matrix equations. In Section III, numerical examples are provided to validate the proposed method by comparing it with the commercial software COMSOL Multiphysics. Finally, conclusions are drawn in Section IV.

II. GOVERNING EQUATIONS

In this section, the 3-D heat conduction equations with different types of boundary conditions are firstly presented and then followed by the finite element formulas of time-domain DDM. The adaptive time step iteration method combined with DDM and its implementation is shown at the end of this section.

A. 3-D HEAT CONDUCTION EQUATIONS

The governing equation of 3-D transient heat conduction is given as:

$$\rho C \frac{\partial T(r,t)}{\partial t} = \nabla \cdot (\kappa(r,T)\nabla T(r,t)) + f(r,t) \tag{1}$$

where ρ, C and $\kappa(r,T)$ represent the mass density, specific heat capacity and thermal conductivity of the material, respectively. $f(r,t)$ denotes the heat excitation changing with position and time, and $T(r,t)$ is the time-varying temperature distribution in the computational domain. Different kinds of boundary conditions are considered in this work [34], [35]:

$$T|_{\Gamma_1} = T_0 \tag{2a}$$

$$\frac{\partial T}{\partial n}|_{\Gamma_2} = 0 \tag{2b}$$

$$\kappa \frac{\partial T}{\partial n}|_{\Gamma_3} = -h_c\,(T - T_{\text{ambient}}) \tag{2c}$$

$$\kappa \frac{\partial T}{\partial n}|_{\Gamma_4} = -\varepsilon_0 \sigma \left(T^4 - T_{\text{ambient}}^4\right) \tag{2d}$$

where Γ_1 represents the Dirichlet boundary and T_0 is the constant of temperature in (2a). Γ_2 is the insulation boundary in (2b) and n is the unit outward normal vector perpendicular to the boundary surface. Γ_3 is the natural convection boundary, h_c and T_{ambient} denote the convective heat transfer coefficient and ambient temperature, respectively in (2c). Γ_4 presents the radiation boundary, where ε_0 and σ are the surface emissivity and the Stefan-Boltzmann constant, respectively in (2d). Moreover, the 3-D transient heat conduction

equation with a given initial temperature distribution:

$$T(r, t = 0) = T_{\text{initial}} \tag{3}$$

B. DDM DISCRETIZED SYSTEM

Here, we discuss the spatial discretization of DDM for 3-D multiscale structures. Assuming the computational domain is divided into N non-overlapping subdomains, nonconforming meshes are employed on the interfaces between different subdomains. Meanwhile, in order to communicate fields between adjacent subdomains, the continuities of temperature and heat flux are needed to guarantee [36], [37]. Taking the i-th subdomain as the local subdomain and assuming it is adjacent to the j-th subdomain, the interface values of heat flux and temperature should, respectively, satisfy:

$$-\kappa^{(i)}\frac{\partial T^{(i)}}{\partial n^{(i)}} = \kappa^{(j)}\frac{\partial T^{(j)}}{\partial n^{(j)}} \tag{4}$$

$$T^{(i)} = T^{(j)} \tag{5}$$

and the governing equations in the $i-$ th domain can be described as:

$$\rho^{(i)}C^{(i)}\frac{\partial T^{(i)}}{\partial t} = \nabla\cdot(\kappa^{(i)}\nabla T^{(i)}) + f^{(i)}, \quad i = 1, 2, \cdots, N \tag{6}$$

then, the following residual expressions are:

$$R_{\Omega^{(i)}} = \rho^{(i)}C^{(i)}\frac{\partial T^{(i)}}{\partial t} - \nabla\cdot(\kappa^{(i)}\nabla T^{(i)}) - f^{(i)} \tag{7a}$$

$$2R^{(i)}_{\Gamma_{ij}}|_q = -\kappa^{(j)}\frac{\partial T^{(j)}}{\partial n^{(j)}} - \kappa^{(i)}\frac{\partial T^{(i)}}{\partial n^{(i)}} \tag{7b}$$

$$R^{(i)}_{\Gamma_{ij}}|_T = \delta\left(T^{(j)} - T^{(i)}\right) \tag{7c}$$

where Γ_{ij} means the interface between the subdomain i and j $(i, j = 1, 2, \cdots, N)$. $R_{\Omega^{(i)}}$ represents the residual of subdomain i. $R^{(i)}_{\Gamma_{ij}}|_q$ and $R^{(i)}_{\Gamma_{ij}}|_T$ denote the jump for the heat flux and temperature. δ is called as the stability coefficient which is related to the mesh feature size and thermal conductivity [19], [35]. By applying the Galerkin method, the weak form of (6) is obtained as follows:

$$\begin{aligned}\int_{\Omega^{(i)}} W_k^{(i)}\cdot\rho^{(i)}C^{(i)}\frac{\partial T^{(i)}}{\partial t}d\Omega^{(i)} &- \int_{\Omega^{(i)}} W_k^{(i)}\cdot\nabla\cdot(\kappa^{(i)}\nabla T^{(i)})d\Omega^{(i)} \\ &- \int_{\Omega^{(i)}} W_k^{(i)}\cdot f^{(i)}d\Omega^{(i)} = 0\end{aligned} \tag{8}$$

where $W_k^{(i)}$ is the $k-$ th test function in the i-th subdomain. Employing Green's identity, equation (8) can be converted into:

$$\begin{aligned}\int_{\Omega^{(i)}} W_k^{(i)}\cdot\rho^{(i)}C^{(i)}\frac{\partial T^{(i)}}{\partial t}d\Omega^{(i)} &+ \int_{\Omega^{(i)}}\nabla W_k^{(i)}\cdot\kappa^{(i)}\nabla T^{(i)}d\Omega^{(i)} \\ &- \int_{\partial\Omega^{(i)}} W_k^{(i)}\cdot n\cdot\kappa^{(i)}\nabla T^{(i)}dS^{(i)} \\ &- \int_{\Omega^{(i)}} W_k^{(i)}\cdot f^{(i)}d\Omega^{(i)} = 0\end{aligned} \tag{9}$$

Finally, by considering the different boundary conditions, the weak formulation of the i-th region yields:

$$\begin{aligned}\int_{\Omega^{(i)}} W_k^{(i)}\cdot\rho^{(i)}C^{(i)}\frac{\partial T^{(i)}}{\partial t}d\Omega^{(i)} &+ \int_{\Omega^{(i)}}\nabla W_k^{(i)}\cdot\kappa^{(i)}\nabla T^{(i)}d\Omega^{(i)} \\ &+ \int_{\Gamma_3} W_k^{(i)}\cdot h_c(T^{(i)} - T_{\text{ambient}})d\Gamma_3 \\ &+ \int_{\Gamma_4} W_k^{(i)}\cdot\varepsilon_0\sigma({T^{(i)}}^4 - T^4_{\text{ambient}})d\Gamma_4 \\ &+ \int_{\Gamma_{ij}} W_k^{(i)}\cdot\delta(T^{(i)} - T^{(j)})d\Gamma_{ij} \\ &- \int_{\Omega^{(i)}} W_k^{(i)}\cdot f^{(i)}d\Omega^{(i)} = 0\end{aligned} \tag{10}$$

In this work, the first-order nodal basis functions of tetrahedron elements are selected for spatial discretization, and the spatially discrete linear equations of the i-th subdomain can be written as:

$$M^{(i)}\frac{d\tilde{T}^{(i)}}{dt} = \sum_{j=1}^{N} L^{(ij)}\tilde{T}^{(j)} + F^{(i)}, \quad i = 1, 2, \ldots N \tag{11}$$

where $\tilde{T}^{(i)}$ denotes the coefficient vector of the discretized temperature in $\Omega^{(i)}$, $M^{(i)}$ is the damping matrix, $L^{(ii)}$ includes the stiffness matrix and the surface integrations in the i-th subdomain. $L^{(ij)}$ $(i \neq j)$ represents the coupled matrix that extracts the interface integrations between the i-th subdomain and the j-th adjacent subdomain. $F^{(i)}$ is the heat excitation vector of the i-th subdomain. Formulations of the above matrices and vectors are as follows:

$$[M^{(i)}]_{kl} = \int_{\Omega^{(i)}} W_k^{(i)}\cdot\rho^{(i)}C^{(i)}W_l^{(i)}d\Omega \tag{12}$$

$$\begin{aligned}[L^{(ii)}]_{kl} = &\int_{\Omega^{(i)}}\nabla W_k^{(i)}\cdot\kappa^{(i)}\nabla W_l^{(i)}d\Omega \\ &+ h_c\int_{\Gamma_3} W_k^{(i)}\cdot W_l^{(i)}d\Gamma_3 + \delta\int_{\Gamma_{ij}} W_k^{(i)}\cdot W_l^{(i)}d\Gamma_{ij},\end{aligned} \tag{13}$$

$$[L^{(ij)}]_{kl} = \delta\int_{\Gamma_{ij}} W_k^{(i)}\cdot W_l^{(j)}d\Gamma_{ij}, \ i \neq j \tag{14}$$

$$\begin{aligned}[F^{(i)}]_k = &\int_{\Omega^{(i)}} W_k^{(i)}\cdot f^{(i)}d\Omega - h_c\int_{\Gamma_3} W_k^{(i)}\cdot T_{\text{ambient}}d\Gamma_3 \\ &+ \varepsilon_0\sigma\int_{\Gamma_4} W_k^{(i)}\cdot(\tilde{T}^{(i)^4} - T^4_{\text{ambient}})d\Gamma_4\end{aligned} \tag{15}$$

C. TEMPORAL DISCRETIZATION AND ADAPTIVE TIME STEP

In the difference approximation method, the time derivative of temperature field T can be approximated in a finite difference form:

$$(1-\alpha)\frac{d\tilde{T}^{(i)}_n}{dt} + \alpha\frac{d\tilde{T}^{(i)}_{n+1}}{dt} = \frac{\tilde{T}^{(i)}_{n+1} - \tilde{T}^{(i)}_n}{\Delta t_n} \tag{16}$$

for $0 \leq \alpha \leq 1$ and a sufficiently small-time step Δt_n, where n and $(n+1)$ represent the last n-th step and present $(n+1)$-th step, respectively, and Δt_n is the time interval. Setting $\alpha = 0$, the forward difference (11) can be obtained:

$$M^{(i)}\frac{d\tilde{T}_n^{(i)}}{dt} = M^{(i)}\frac{\tilde{T}_{n+1}^{(i)} - \tilde{T}_n^{(i)}}{\Delta t_n} = \sum_{j=1}^{N} L^{(ij)}\tilde{T}_n^{(j)} + F_n^{(i)} \quad (17)$$

Writing the discrete equation in a matrix form with:

$$A_{\text{forward}}^{(i)} = M^{(i)} \quad (18a)$$

$$b_{\text{forward}}^{(i)} = M^{(i)}\tilde{T}_n^{(i)} + \Delta t_n \sum_{j=1}^{N} L^{(ij)}\tilde{T}_n^{(j)} + \Delta t_n F_n^{(i)} \quad (18b)$$

At the same time, letting $\alpha = 1$, the backward difference equation can be written as:

$$M^{(i)}\frac{d\tilde{T}_{n+1}^{(i)}}{dt} = M^{(i)}\frac{\tilde{T}_{n+1}^{(i)} - \tilde{T}_n^{(i)}}{\Delta t} = \sum_{j=1}^{N} L^{(ij)}\tilde{T}_{n+1}^{(j)} + F_{n+1}^{(i)} \quad (19)$$

the corresponding matrix form is denoted as:

$$A_{\text{backward}}^{(i)} = M^{(i)} - \Delta t_n L^{(ii)} \quad (20a)$$

$$b_{\text{backward}}^{(i)} = M^{(i)}\tilde{T}_n^{(i)} + \Delta t_n \sum_{j=1, j\neq i}^{N} L^{(ij)}\tilde{T}_{n+1}^{(j)} + \Delta t_n F_{n+1}^{(i)} \quad (20b)$$

To ensure stability in solving the transient thermal field equations, especially for the explicit iteration method, the relationship between the time step Δt_n and the mesh size h must follow the rule [38]: $l_{\text{diffusion}} \sim \sqrt{D\Delta t_n}$, where $D = \kappa/\rho C$ is the thermal diffusion coefficient, $l_{\text{diffusion}}$ represents the thermal diffusion length. In terms of discrete mesh, $h = \sqrt{l_{\text{diffusion}}/6}$ are required in thermal diffusion length [39], [40].

For the sake of improving the computation speed, the adaptive time step is preferred in this work in terms of its ability to automatically control the time interval Δt_n by the error of two adjacent iterations between the correction term and the prediction term. The formula in [41] is given as:

$$d(\tilde{T}_{n+1}^{(i)}) = \frac{\max(\tilde{T}_{n+1}^{(i)} - \tilde{T}_{n+1}^{(i),p})}{2} + O(\Delta t_n)^3 \quad (21a)$$

$$\Delta t_{n+1} = \Delta t_n \left(\frac{\varepsilon}{\left|d\left(\tilde{T}_{n+1}^{(i)}\right)\right|}\right)^{\frac{1}{3}} \quad (21b)$$

where ε is the threshold of the control step which effects numerical accuracy and CPU time. It is set as 10^{-3} in this work. To simplify the temporal discretization, the forward difference is used to obtain the prediction term $\tilde{T}_{n+1}^{(i),p}$ and the implicit backward Euler difference is employed to get the correction term $\tilde{T}_{n+1}^{(i)}$. Every mesh cell in the same subdomain uses the same adaptive time step. At the same time, the same time step is also employed for different subdomains. The term $\max(\tilde{T}_{n+1}^{(i)} - \tilde{T}_{n+1}^{(i),p})$ in (21a) describes the maximum error within all subdomains. Then the adaptive time step depends is the smallest one of the subdomains.

To clearly demonstrate the adaptive time iteration, the corresponding pseudo-code is given as follows:

```
while error > ε
 for i = 1 : N
    A^(i)_backward = M^(i) − Δt_n L^(ii)
    b^(i)_backward = M^(i) T̃^(i)_n + Δt_n F^(i)_{n+1}
  for j = 1 : i − 1
    b^(i)_backward = b^(i)_backward + Δt_n L^(ij) T̃^(j)_{n+1}
  end
  for j = i + 1 : N                                          (22)
    b^(i)_backward = b^(i)_backward + Δt_n L^(ij) T̃^(j)_{n+1}
  end
  solve A^(i)_backward T̃^(i)_{n+1} = b^(i)_backward
 end
execute (21)
error = max(‖ T̃^(i)_{n+1} − T̃^(i),p_{n+1} ‖ / ‖ T̃^(i)_{n+1} ‖)
end
```

```
for endtime < total time
  for i = 1 : N
    A^(i)_forward = M^(i)
    b^(i)_forward = M^(i) T̃^(i)_n + Δt_n F^(i)_n
    for j = 1 : N
      b^(i)_forward = b^(i)_forward + Δt_n L^(ij) T̃^(j)_n     (23)
    end
    solve A^(i)_forward T̃^(i),p_{n+1} = b^(i)_forward
  end
  execute (22) to update Δt_{n+1}
  endtime = endtime + Δt_{n+1}
end
```

The processing of the time iteration is shown in (22), and the (22) is a loop in (23). By combining (22) as a loop in (23) we can update each time step according to the error between the correction term and the prediction term. In the time discretization, the thermal radiation boundary condition $\int_{\Gamma_4} W_k^{(i)} \cdot (\tilde{T}^{(i)^4} - T_{\text{ambient}}^4) d\Gamma_4$ in (15) is a nonlinear term. In order to avoid the complexity of solving the nonlinear equation, the temperature field of the n-th step $T_n^{(i)}$ is used by $F_n^{(i)}$ in (22).

III. NUMERICAL RESULTS AND DISCUSSION

To verify the feasibility, accuracy, as well as stability of the proposed DDM with the adaptive time step algorithm, several representative examples are investigated in this section. Meanwhile, to characterize the error between the proposed method and the reference solution, relative error in L_2 norm is defined as:

$$\text{Error} = \|T_{\text{DDM}} - T_{\text{ref}}\| \,/\, \|T_{\text{ref}}\| \quad (24)$$

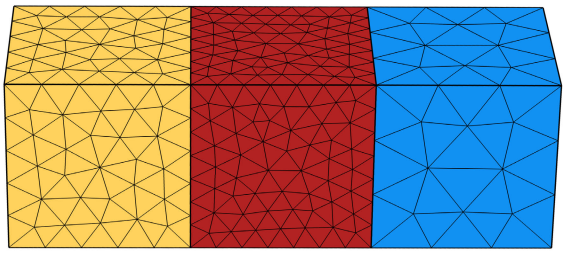

FIGURE 1. A rectangular silicon brick model is divided into three different subdomains for DDM implementation.

where T_{DDM} denotes the solution obtained from the proposed method, T_{ref} represents the analytical solution or the reference solution by the FEM commercial software COMSOL Multiphysics.

It is important to note that the proposed method and COMSOL are using different meshes in this work. COMSOL employs the conformal tetrahedral meshes, while the proposed method utilizes non-conformal meshes. For each numerical case, the convergent meshes need to be verified first. Based on this, the finer meshes are used in COMSOL to obtain the reference solutions. To compare time consumption between the proposed method and COMSOL, a similar number of COMSOL mesh is also employed. Meanwhile, based on the multiscale models and their different medium of each subdomain, different meshing densities are obtained to meet the thermal diffusion conditions. Currently, the proposed method is coded and implemented in a single computer with Intel(R) Core(TM) i7-7700 CPU (3.60 GHz,12-GB memory).

A. SILICON BRICK

Firstly, the transient thermal profile of a rectangular silicon brick is studied, and the calculated numerical results are compared with its exact solutions [25]. The silicon brick with dimensions 1 m × 1 m × 3 m is divided into three different subdomains at $z = 1$ m and $z = 2$ m by the non-conformal and independent meshes as shown in Fig.1. The Dirichlet boundary conditions are set with $T(x, y, z = 0; t) = T(x, y, z = L; t) = 0$, where $L = 3$ m is the length of the model in the z direction, and the remaining four surfaces are the default thermal insulation boundary conditions. When the initial condition is set as $T(x, y, z; t = 0) = \sin(\pi z/L)$, the corresponding analytical solution is obtained:

$$T(x, y, z; t) = \sin(\frac{\pi z}{L})\exp(-\frac{k\pi^2 t}{\rho C L^2}) \tag{25}$$

The transient temperatures of three different points $\mathrm{R}_1 = (0.5, 0.5, 0.5)$ m, $\mathrm{R}_2 = (0.35, 0.4, 1.5)$ m and $\mathrm{R}_3 = (0.38, 0.1, 2.7)$ m in the silicon brick are shown in Fig. 2 with the stability coefficient $\delta = 10^4$. To verify the accuracy of the proposed method, the corresponding exact solutions by (25) are presented as well. Good agreements between numerical solutions and analytical solutions are obtained in Fig. 2. The relative errors for the three different points are 1.28%, 1.19%, 1.64%, respectively. Meanwhile, in order to clearly

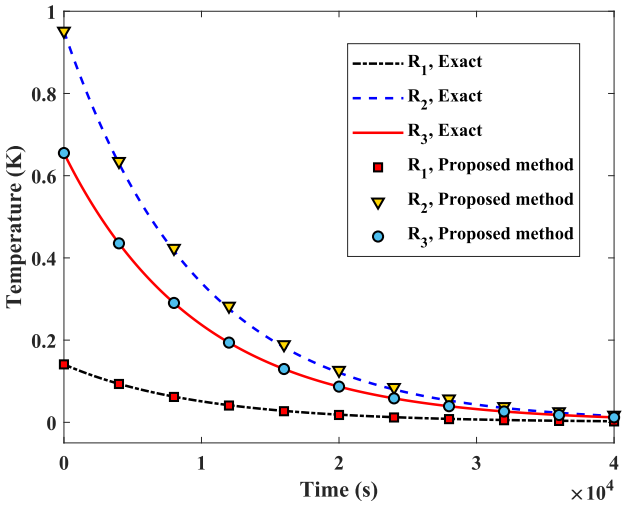

FIGURE 2. Comparison of the calculated temperature T at three different locations R_1, R_2, R_3 between the proposed method (markers) and the exact solution (lines).

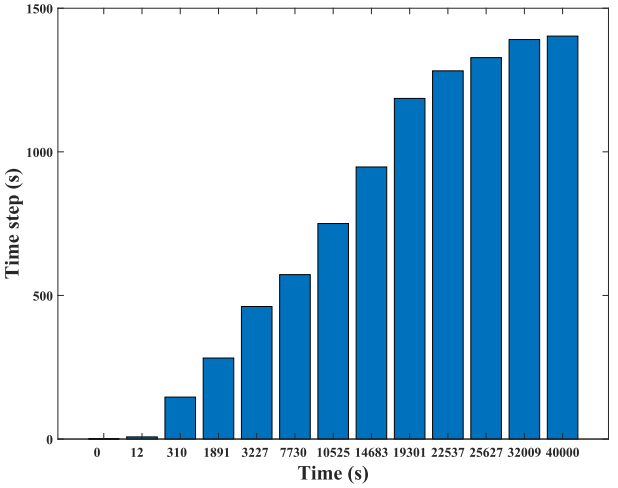

FIGURE 3. The nonuniform time steps obtained from the proposed method.

show the time steps obtained by the adaptive time algorithms, illustrative time steps selected by uniformly sampling (every seven iterations) are presented in Fig. 3. It shows that the time steps are automatically determined by the evolution of the temperature fields in Fig. 2. That is, the time intervals are smaller when the temperature fields change rapidly. While when the temperature asymptotically approaches the steady state as the time evolves, the time intervals become larger. Table 1 compares the computational costs and time interval values of the proposed method with COMSOL under a similar amount of DoFs and conformal meshes. The computational cost is mainly spent on the mesh pre-processing, assembling and solving of discrete matrix. The CPU time for post-processing plot of each point is much less than the previous calculation time. Therefore, the computational costs for point R_1, R_2 and R_3 are almost the same, then only the computational cost of R_1 is shown in Table 1. From this table,

TABLE 1. Time step values, cpu time and relative errors in proposed method and COMSOL for silicon brick.

Method	DoFs	Time step (s)	Total time (s)	CPU time (s)	Error
COMSOL	2,124	0.5	40,000	737	1.30%
Proposed method	2,129	0.5∼1403	40,000	18	1.28%

TABLE 2. Material parameters of the thermoelectric cooler case.

Materials	κ (W/[m · K])	C (J/[kg · K])	ρ (kg/m^3)
Bi_2Te_3, P-type	1.62	154	7,700
Bi_2Te_3, N-type	$\kappa(T)$ in Fig. 4(b)	154	7,700
Tungsten	175	132	17,800
Copper	400	385	8,960

we note that compared with COMSOL using the fixed time step, the proposed method shows significant improvement in total CPU time (approximately 40 times). It clearly illustrates that the new method can remarkably boost the computational speed and economize the computational costs as same level of accuracy is achieved.

B. THERMOELECTRIC COOLER

Thermoelectric coolers are widely used in a variety of applications ranging from consumer products to high-temperature electronics equipment. They consist of multiple thermoelectric arms sandwiched between two heat-conducting plates with one side cool and the other side heat [42]. The 2-D cross-sectional view of a thermoelectric cooler is shown in Fig. 4(a). Due to the use of temperature-dependent material Bi_2Te_3 (N-type), its thermal conductivity changes nonlinearly with temperature as presented in Fig. 4(b). The corresponding material parameters of the model are shown in Table 2.

Based on the layered feature of the structure, the model is naturally divided into five subdomains with independent meshes from top to bottom, which are the upper Tungsten layer, the upper copper layer, the Bi_2Te_3 layer, the lower cooper layer, and the lower Tungsten layer. The number of tetrahedron elements in each subdomain is 1,741, 8,423, 30,264, 5,915 and 3,408, respectively, and the corresponding DoFs of each subdomain are 637, 3,209, 7,170, 2,337 and 1,194, respectively. Considering the device is driven by an electrical signal of periodic sine waveform, the power consumption on the top layer is set as $P_1 = 0.5\sin(0.035t) + 0.5$ W with an isotherm boundary 293.15 K at the bottom of the cooler [22]. The surroundings are thermal insulation boundary conditions. Meanwhile, the initial temperature distribution is set to 293.15 K throughout the whole system.

The 3-D temperature distribution at $t = 100$ s obtained by the proposed method is shown in Fig. 5(a), and the corresponding 2-D cross-section temperature distribution at $x = 1$ mm is plotted in Fig. 5(b). It can be seen that the heat is effectively transferred from the upper side to the lower layer and the temperature distribution is smooth across different subdomains. The upper part of the cooler has

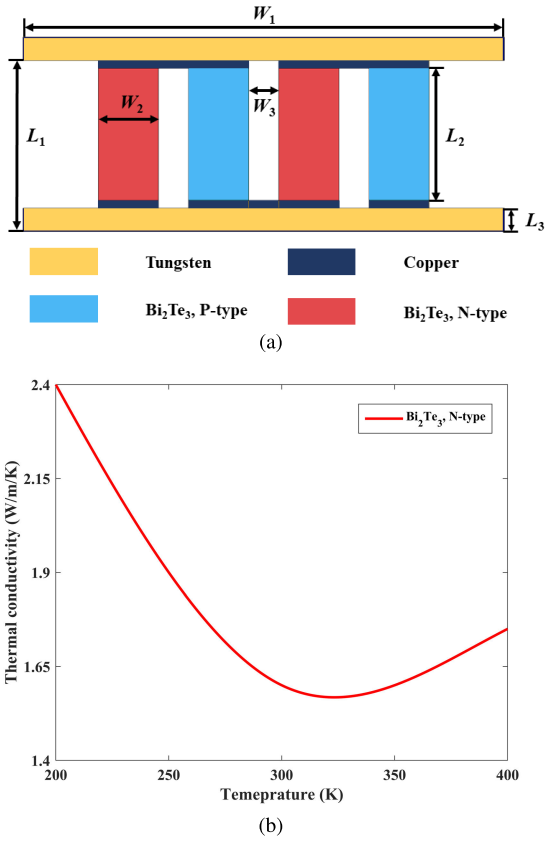

FIGURE 4. Cross-sectional view and material characteristics of the thermoelectric cooler: (a) Cross-sectional view, (b) Nonlinear thermal conductivity of Bi_2Te_3 (N-type). The geometrical parameters are given as $W_1 = 8$ mm, $W_2 = 1$ mm, $W_3 = 0.5$ mm, $L_1 = 2.2$ mm, $L_2 = 1.7$ mm, $L_3 = 0.3$ mm.

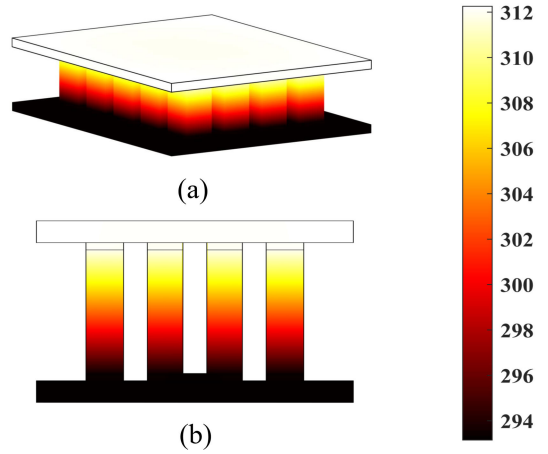

FIGURE 5. Temperature distribution of the thermoelectric cooler at time $t = 100$ s: (a) 3-D temperature distribution, (b) Snapshot of the temperature profile on YZ plane with $x = 1$ mm.

a higher temperature distribution, while the temperature of the bottom layer is accordant with the boundary condition with $T = 293.15$ K.

To further verify the accuracy of the simulation results, the transient temperatures at two different observation points $R_1 = (1.5, 0.98, 2.3)$ mm and $R_2 = (2.2, 1.5, 1)$ mm,

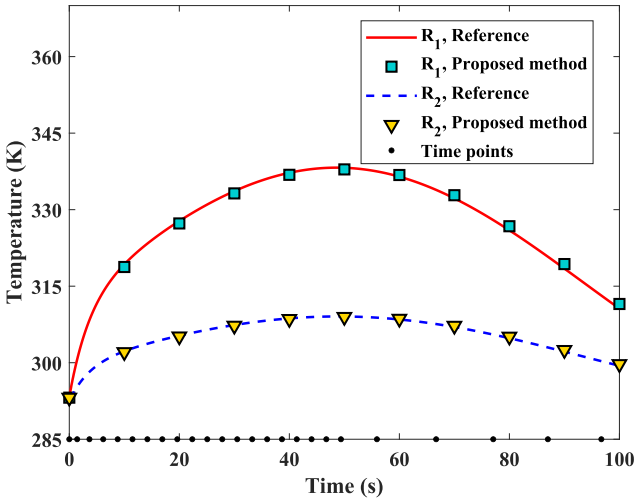

FIGURE 6. Transient temperatures at points R_1 and R_2 by the proposed method. References are obtained by COMSOL with 78,931 DoFs.

TABLE 3. Time step values, cpu time, and relative errors in proposed method and COMSOL for the thermoelectric cooler.

Method	DoFs	Time step (s)	Total time (s)	CPU time (s)	Error
COMSOL	14,552	0.1	100	267	0.04%
Proposed method	14,547	0.1∼1.12	100	162	0.07%

which are located in the upper layer and the thermoelectric arm, are given in Fig. 6, respectively. The references obtained by COMSOL with a larger amount of DoFs (78,931) are also presented in this figure. Excellent agreements are obtained between the proposed method and the references with the relative errors being 0.17% for R_1 and 0.07% for R_2, respectively. The time step values, the CPU time costs, and relative errors by the proposed method and by COMSOL with a similar amount of DoFs are also investigated in Table 3. By utilizing the automatically adaptive step size algorithm as shown in Fig. 6, the CPU time of the proposed method is reduced by 39% compared to COMSOL, which proves that the proposed algorithm is as well suitable for the 3-D complex structure with temperature-dependent materials.

C. BANDPASS FILTER BASED ON LTCC

Low-temperature cofired ceramic (LTCC) composed of glass and ceramics is widely employed in microelectronic packaging, owing to its high conductivity and low cost. Meanwhile, the multi-layer manufacturing process provides enough space for LTCC to accommodate many resonators. In this subsection, a 3-D compact bandpass filter based on the LTCC module is studied [43], [44]. The filter has four parts that include the LTCC module, the top copper ground plane, the Roger substrate, and the bottom copper ground plane as described in Fig. 7(a). The resonators inside the LTCC module are shown in Fig. 7(b), which consist of four metal layers: the first layer includes the feeding lines, the second and fourth are resonators and the third layer is the ground plane. These

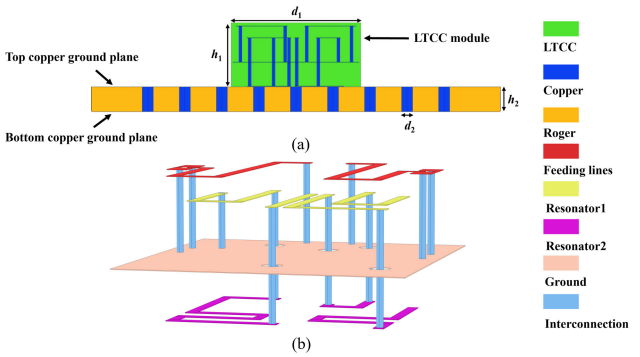

FIGURE 7. (a) Lateral schematic of bandpass filter based on LTCC, (b) 3-D distribution of resonators inside LTCC module.

TABLE 4. Material parameters of the LTCC case.

Materials	κ (W/[m · K])	C (J/[kg · K])	ρ (kg/m^3)
LTCC	3.3	989	3,100
Copper	400	385	8,940
Roger	50	180	9,290

four layers interconnect each other. The height of the LTCC module is $h_1 = 2.1$ mm in Fig. 7 and the length d_1 is 4.2 mm, the height of Roger substrate h_2 equals to 0.83 mm in which contains 34 Copper columns with a diameter of $d_2 = 0.3$ mm. According to the structures in Fig. 7(a), the whole computational domain is divided into the corresponding four subdomains. The number of elements for the proposed DDM are 117,530, 9,408, 13,460 and 9,424, respectively, and with the corresponding DoFs in each subdomain being 162,122, 19,317, 21,704, and 19,282, respectively. Moreover, due to the thin thickness of the ground planes which are only 0.01 mm, high-quality meshing is crucial to accurate numerical results. The thin layers here are divided by aids of the powerful modeling flexibility of DDM, while the mesh densities and DoFs of the rest parts are minimized as much as possible to facilitate calculation. A multi-peak square wave shown in Fig. 8 is set inside the whole LTCC module to act as a heat source. Cooling through convection and radiation takes place at all external boundaries with a heat convective coefficient $h_c = 50$ W/[m^2 · K], a surface emissivity $\varepsilon_0 = 0.93$, and $\sigma = 5.67 \times 10^{-8}$ W/[m^2 · K^4]. Meanwhile, the initial temperature of the whole system is 298.15 K and their material parameters are given in Table 4.

The transient temperature at two observation points $R_1 = (0.75, 0.54, 0)$ mm and $R_2 = (0.22, 0.15, 1)$ mm which are located at Roger substrate and LTCC module are shown in Fig. 9. The temperatures rise and fall twice in the whole activation process which follows the square wave patterns with the peak temperature happening at 75 s and 200 s, respectively. Figure 9 also depicts that the calculation results well agree with the reference solutions from COMSOL. In Fig. 10, the 3-D temperature distributions at 185 s and 190 s are provided by the proposed method where can see the heat transfer inside LTCC. To more clearly observe

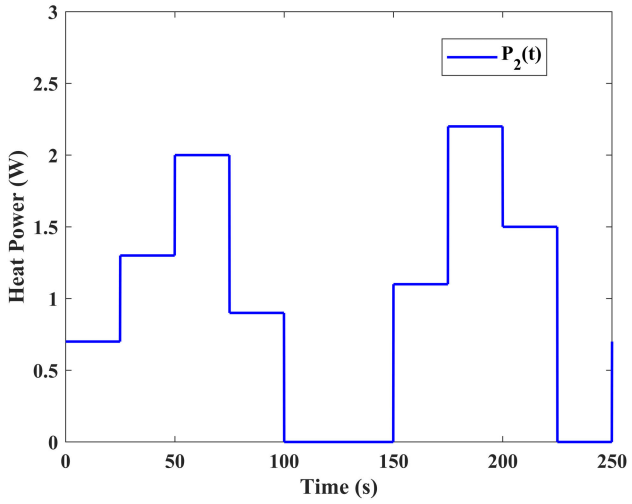

FIGURE 8. The transient curve of the multi-peak square wave $P_2(t)$ of LTCC module.

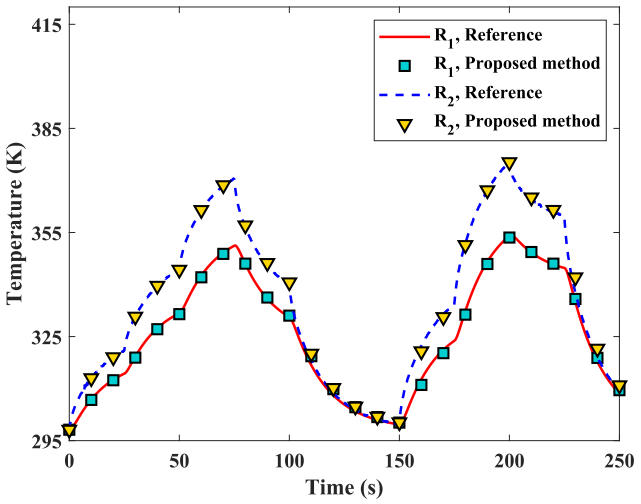

FIGURE 9. Transient temperature at points R_1 and R_2. References are obtained by COMSOL with 952,106 DoFs.

TABLE 5. Time step values, cpu time and relative errors in proposed method and COMSOL for LTCC case.

Methods	DoFs	Time step (s)	Total time (s)	CPU time (s)	Error
COMSOL	201,392	0.1	250	4321	0.07%
Proposed method	222,425	0.1∼1.72	250	1428	0.49%

the transfer, the one side resonators transient temperature fields as shown in Fig. 11 at the different time steps. Taking COMSOL with 952, 106 DoFs as the reference solution, the comparison for the proposed method and COMSOL with less DoFs of 201, 392 is shown in Table 5. The CPU time of the proposed algorithm is reduced by 67% compared with COMSOL under the fixed time step which clearly suggests that the combination of DDM and adaptive time step has an excellent performance.

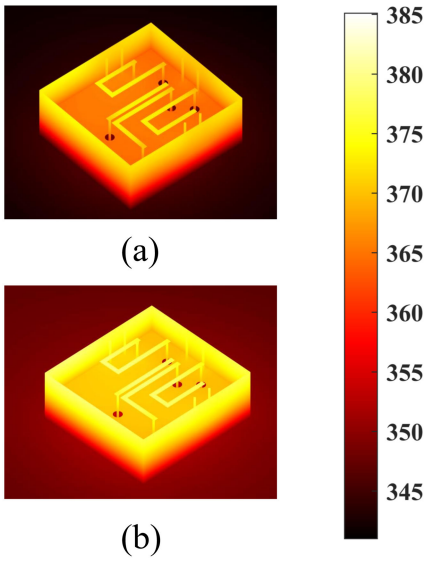

FIGURE 10. The calculated temperature distributions of the LTCC module by the proposed method at (a) t = 185 s, (b) t = 190 s.

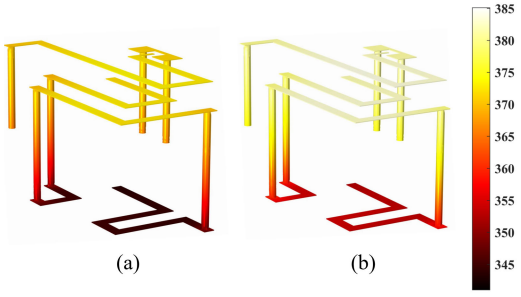

FIGURE 11. 3-D transient temperature of the one side resonators in LTCC module by the proposed method at (a) t = 185 s, (b) t = 190 s.

D. INTEGRATION PACKAGE AND INTERCONNECT

Finally, a 3-D IC package with vertically stacked-up chips connected by TSVs is studied. The multilayer and multiscale integration package shown in Fig. 12 has a similar structure as in [19]. The module is comprised of the heat sink, thermal spreader with 12 thermal vias, memory die with 24 TSVs, two C4 layers and one CPU chip with 54 TSVs whose material parameters are given in Table 6. The height h_1 of the top heat sink is 6.8 mm, the height of h_2 and h_3 are the same, which are equal to 0.5 mm, and $d_3 = 2$ mm. The 3-D structure is divided according to the functional layer into six subdomains which are the heat sink, the thermal spreader layer, the memory chip layer, the upper C4 layer, the CPU chip layer and the bottom C4 layer, respectively. The number of elements in each subdomain is 128,945, 110,927, 436,149, 12,907, 283,136 and 9,728, respectively. The corresponding DoFs are 42,758, 24,776, 79,716, 4,394, 53,390 and 3,292. The heat sources in the CPU and memory chips are in the same forms and distribution in [19]: $Q_1^c = 0.1Q_c$, $Q_2^c = 0.15Q_c$, $Q_3^c = 0.175Q_c$, $Q_4^c = 0.125Q_c$ with $Q_c = |\cos(2\pi y/3l_1)|$. $Q_1^m = 0.3Q_m$, $Q_2^m = 0.35Q_m$, $Q_3^m = 0.325Q_m$, $Q_4^m = 0.315Q_m$ with $Q_m = |\cos(3\pi y/2l_1)|$. $l_1 = 12$ mm is the side

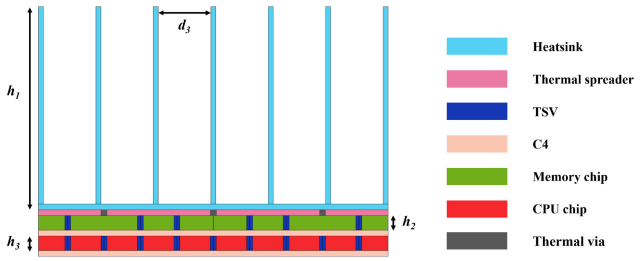

FIGURE 12. Schematic diagram of the investigated 3-D IC package.

TABLE 6. Material parameters of the 3-D IC package.

Materials	k (W/[m · K])	C (J/[kg · K])	ρ (kg/m^3)
Thermal spreader	400	385	8,933
Heat sink	220	896	2,707
Chip die	135	704	2,330
TSV	400	385	8,933
C4	50	180	9,290

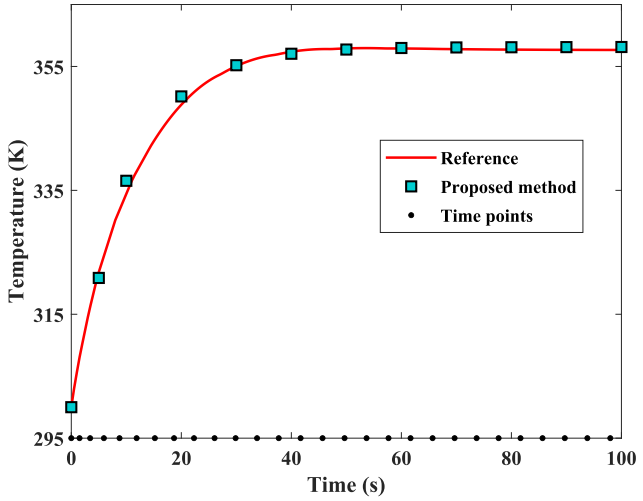

FIGURE 13. Transient temperature at point R. Reference is obtained by COMSOL with 803,409 DoFs.

length of the IC package. The thermal spreader layer is also regarded as a heat source and its power is $P = 3$ W. The heat sink layer has the equivalent convection boundary with $h_c = 50$ W/[m^2 · K] and the surface-to-ambient radiation boundary with $\varepsilon_0 = 0.93$ and $\sigma = 5.67 \times 10^{-8}$ W/[m^2 · K^4].

The transient temperature at the point R $= (-6, -6, -0.1)$ mm placed in the CPU layer is shown in Fig. 13. Compared with the reference obtained by COMSOL of 803, 409 DoFs, the relative error of our proposed method is 0.02%. The 2-D temperature distribution at $x = 0.01$ mm and $t = 100$ s is presented in Fig. 14 when the system is in the stable state, we can see due to the convection and radiation heat transfer by the top radiator, the temperature on the upper part is lower. Putting the COMSOL 803,409 DoFs as the reference solution and comparing the proposed method with the COMSOL results under similar DoFs, the CPU time and time step values are given in Table 7. It clearly demonstrates that the DDM with

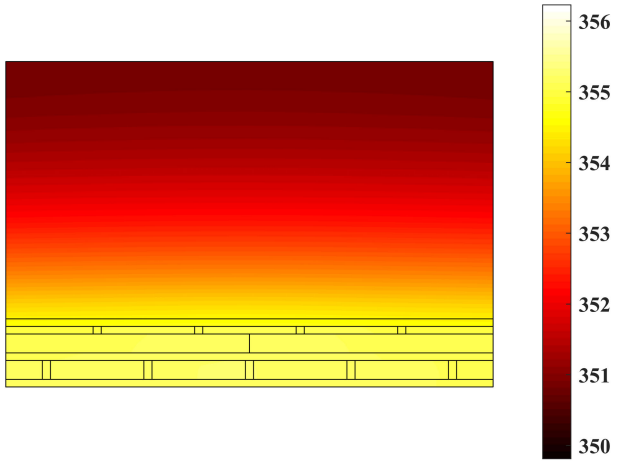

FIGURE 14. Cross-sectional view of temperature distribution on YZ plane at $x = 0.01$ mm and $t = 100$ s.

TABLE 7. Time step values, cpu time and relative errors in proposed method and COMSOL for 3-D IC package.

Methods	DoFs	Time step (s)	Total time (s)	CPU time (s)	Error
COMSOL	204,254	0.5	100	6,761	0.04%
Proposed method	208,326	0.5∼1.05	100	2,129	0.02%

adaptive time step can reduce 68.5% CPU time within the allowable error range, further proving the excellent efficiency and accuracy of the proposed new method.

IV. CONCLUSION

In this work, a DDM algorithm with an adaptive time step is proposed to analyze the thermal behaviors in 3-D IC packages. The numerical cases with heat conduction, convection and radiation boundaries are investigated. The thermal analysis of several 3-D multiscale IC structures is compared with COMSOL results to verify the accuracy and efficiency of the new algorithm. By combing the advantages of DDM and adaptive time step, taking the LTCC case as an example, the efficiency is enhanced by 67% when the relative error is 0.5% compared with the references. The new method can not only flexibly generate meshes for different scales, but also automatically control time steps which significantly speeds up computational efficiency. The thermal analysis of several 3-D multiscale IC structures is compared with COMSOL results to verify the accuracy and efficiency of the new algorithm. Due to its inherently parallel performance, future work will focus on parallelizing the codes at a subdomain level and thermo-mechanical multi-physics analysis. With all of these performances and improvements, we anticipate that the proposed method can be utilized routinely to simulate the dynamic thermal analysis of 3-D ICs.

REFERENCES

[1] S. G. Kandlikar, "Review and projections of integrated cooling systems for three-dimensional integrated circuits," *J. Electron. Packag.*, vol. 136, no. 2, Jun. 2014, Art. no. 024001.

[2] S. S. Salvi and A. Jain, "A review of recent research on heat transfer in three-dimensional integrated circuits (3-D ICs)," *IEEE Trans. Compon., Packag., Manuf. Technol.*, vol. 11, no. 5, pp. 802–821, Mar. 2021.

[3] J. U. Knickerbocker, "3-D silicon integration and silicon packaging technology using silicon through-vias," *IEEE J. Solid-State Circuits*, vol. 41, no. 8, pp. 1718–1725, Aug. 2006.

[4] A. Jain, R. E. Jones, R. Chatterjee, and S. Pozder, "Analytical and numerical modeling of the thermal performance of three-dimensional integrated circuits," *IEEE Trans. Compon. Packag. Technol.*, vol. 33, no. 1, pp. 56–63, Mar. 2010.

[5] L. P. M. Colombo, D. Paleari, and A. Petrushin, "A model of BGA thermal vias as an example of lumped parameter analysis in thermal modeling of SiPs and stacked die packages," *Proc. IEEE*, vol. 97, no. 1, pp. 70–77, Jan. 2009.

[6] H. Kock, S. Eiser, and M. Kaltenbacher, "Electrothermal multiscale modeling and simulation concepts for power electronics," *IEEE Trans. Electron Devices*, vol. 57, no. 1, pp. 345–352. Jan. 2010.

[7] P. Srikrishna, T. Chanakya, R. Venkateswaran, P. R. R. Rao, and S. K. Datta, "Thermal analysis of high-average power helix traveling-wave tube," *IEEE Trans. Electron Devices*, vol. 65, no. 6, pp. 2218–2226, Jun. 2018.

[8] C. C. Lee, A. L. Palisoc, and J. M. W. Baynham, "Thermal analysis of solid-state devices using the boundary element method," *IEEE Trans. Electron Devices*, vol. ED-35, no. 7, pp. 1151–1153, Jul. 1988.

[9] R. T. Haftka and D. S. Malkus, "Calculation of sensitivity derivatives in thermal problems by finite differences," *Int. J. Numer. Methods Eng.*, vol. 17, no. 12, pp. 1811–1821, Dec. 1981.

[10] Z. Liu, S. Swarup, S. X.-D. Tan, H.-B. Chen, and H. Wang, "Compact lateral thermal resistance model of TSVs for fast finite-difference based thermal analysis of 3-D stacked ICs," *IEEE Trans. Comput.-Aided Design Integr. Circuits Syst.*, vol. 33, no. 10, pp. 1490–1502, Oct. 2014.

[11] J. N. Reddy and D. K. Gartling, *The Finite Element Method in Heat Transfer and Fluid Dynamics*. Boca Raton, FL, USA: CRC Press, Apr. 2010, pp. 1–489.

[12] L. Xu, P. Xie, S.-Y. Yang, J.-H. Yin, Z.-H. Yang, and B. Li, "Accurate and fast thermal analysis of multistage depressed collectors for traveling-wave tubes using finite-element method," *IEEE Trans. Electron Devices*, vol. 67, no. 2, pp. 690–696, Feb. 2020.

[13] Z. Ren, W. Y. Yin, Y. B. Shi, and Q. H. Liu, "Thermal accumulation effects on the transient temperature responses in LDMOSFETs under the impact of a periodic electromagnetic pulse," *IEEE Trans. Electron Devices*, vol. 57, no. 1, pp. 345–352, Jan. 2010.

[14] Y.-B. Shi, W.-Y. Yin, J.-F. Mao, P. Liu, and Q. H. Liu, "Transient electrothermal analysis of multilevel interconnects in the presence of ESD pulses using the nonlinear time-domain finite-element method," *IEEE Trans. Electromagn. Compat.*, vol. 51, no. 3, pp. 774–783, Sep. 2009.

[15] Y. L. Dong, M. Tang, P. Li, and J. F. Mao, "Transient electromagnetic-thermal simulation of dispersive media using DGTD method," *IEEE Trans. Electromagn. Compat.*, vol. 61, no. 4, pp. 1305–1313, Aug. 2019.

[16] P. Xie, L. Xu, J.-H. Yin, H. Wang, Z.-H. Yang, and B. Li, "An interior penalty domain decomposition method for thermal analysis of 3-D integrated systems," *IEEE Trans. Compon., Packag., Manuf. Technol.*, vol. 11, no. 3, pp. 395–406, Mar. 2021.

[17] H. H. Zhang, "Parallel higher order DGTD and FETD for transient electromagnetic-circuital-thermal co-simulation," *IEEE Trans. Microw. Theory Techn.*, vol. 70, no. 6, pp. 2935–2947, Jun. 2022.

[18] H. X. Zhang, Q. Zhan, L. Huang, Y. D. Wang, W. J. Wang, Z. Qin, Z. G. Zhao, D. W. Wang, H. J. Zhou, K. Kang, L. Zhou, and W. Y. Yin, "A scalable HPC-based domain decomposition method for multiphysics modeling of RF devices," *IEEE Trans. Compon., Packag., Manuf. Technol.*, vol. 11, no. 2, pp. 203–211, Feb. 2020.

[19] P. Li, Y. Dong, M. Tang, J. Mao, L. J. Jiang, and H. Bagci, "Transient thermal analysis of 3-D integrated circuits packages by the DGTD method," *IEEE Trans. Compon., Packag., Manuf. Technol.*, vol. 7, no. 6, pp. 862–871, Jun. 2017.

[20] J. Chen and Q. H. Liu, "Discontinuous Galerkin time-domain methods for multiscale electromagnetic simulations: A review," *Proc. IEEE*, vol. 101, no. 2, pp. 242–254, Feb. 2013.

[21] B. Li, M. Tang, H. Yue, Y. Tang, and J. Mao, "Efficient transient thermal simulation of ICs and packages with laguerre-based finite-element method," *IEEE Trans. Compon., Packag., Manuf. Technol.*, vol. 10, no. 12, pp. 2158–2170, Dec. 2021.

[22] T. Lu and J.-M. Jin, "Transient electrical-thermal analysis of 3-D power distribution network with FETI-enabled parallel computing," *IEEE Trans. Compon., Packag., Manuf. Technol.*, vol. 4, no. 10, pp. 1684–1695, Oct. 2014.

[23] S. Dosopoulos and J.-F. Lee, "Interior penalty discontinuous Galerkin method for the time-domain Maxwell's equations," *IEEE Trans. Magn.*, vol. 46, no. 8, pp. 3512–3515, Aug. 2010.

[24] Y. Shao, Z. Peng, and J.-F. Lee, "Thermal-aware DC IR-drop co-analysis using non-conformal domain decomposition methods," *Proc. Roy. Soc. A, Math., Phys. Eng. Sci.*, vol. 468, no. 2142, pp. 1652–1675, Jun. 2012.

[25] Y. Shao, Z. Peng, and J. F. Lee, "Thermal analysis of high-power integrated circuits and packages using nonconformal domain decomposition method," *IEEE Trans. Compon., Packag., Manuf. Technol.*, vol. 3, no. 8, pp. 1321–1331, Aug. 2013.

[26] J. Chai, G. Dong, and Y. Yang, "Nonlinear electrothermal model for investigating transient temperature responses of a through-silicon via array applied with Gaussian pulses in 3-D IC," *PIEEE Trans. Electron Devices*, vol. 468, no. 2142, pp. 1652–1675, Jun. 2012.

[27] H. H. Zhang, P. P. Wang, S. Zhang, L. Li, P. Li, W. E. I. Sha, and L. J. Jiang, "Electromagnetic-circuital-thermal multiphysics simulation method: A review," *Prog. Electromagn. Res.*, vol. 169, pp. 87–101, 2020.

[28] W. N. Fu and S. L. Ho, "Elimination of nonphysical solutions and implementation of adaptive step size algorithm in time-stepping finite-element method for magnetic field–circuit–motion coupled problems," *IEEE Trans. Magn.*, vol. 46, no. 1, pp. 29–38, Jan. 2010.

[29] Y. Cai, X. Peng, Q. Li, K. Wang, X. Qin, and R. Guo, "The numerical solution of space-dependent neutron kinetics equations in hexagonal-z geometry using backward differentiation formula with adaptive step size," *Ann. Nucl. Energy*, vol. 128, pp. 203–208, Jun. 2019.

[30] C. Ge, B. Duan, S. Lou, S. Qian, and W. Wang, "On improving convergence characterization to solve the electromagnetic–thermal model," *IEEE Trans. Microw. Theory Techn.*, vol. 69, no. 8, pp. 3624–3634, Aug. 2021.

[31] P. M. Gresho, D. F. Griffiths, and D. J. Silvester, "Adaptive time-stepping for incompressible flow—Part I: Scalar advection-diffusion," *SIAM J. Sci. Comput.*, vol. 30, no. 4, pp. 2018–2054, Jan. 2008.

[32] A. A. Rabello, E. J. Silva, R. R. Saldanha, C. Vollaire, and A. Nicolas, "Adaptive time-stepping analysis of nonlinear microwave heating problems," *IEEE Trans. Magn.*, vol. 41, no. 5, pp. 1584–1587, May 2005.

[33] C. Zhang, M. Mihajlovic, and V. F. Pavlidis, "Adaptive transient leakage-aware linearised model for thermal analysis of 3-D ICs," in *Proc. Design, Autom. Test Eur. Conf. Exhib. (DATE)*, Mar. 2019, pp. 268–271.

[34] N. Li, J. Mao, W.-S. Zhao, M. Tang, W. Chen, and W.-Y. Yin, "Electrothermal cosimulation of 3-D carbon-based heterogeneous interconnects," *IEEE Trans. Compon., Packag., Manuf. Technol.*, vol. 6, no. 4, pp. 518–526, Apr. 2016.

[35] D. H. Liu, X. P. Zheng, and Y. H. Liu, "A discontinuous Galerkin finite element method for heat conduction problems with local high gradient and thermal contact resistance," *Comput. Model. Eng. Sci.*, vol. 39, no. 3, pp. 263–299, Jan. 2009.

[36] H. H. Zhang, W. E. I. Sha, Z. X. Huang, and G. M. Shi, "Flexible and accurate simulation of radiation cooling with FETD method," *Sci. Rep.*, vol. 8, no. 1, p. 2652, Feb. 2018.

[37] J. Xie and M. Swaminathan, "3D transient thermal solver using non-conformal domain decomposition approach," in *Proc. IEEE/ACM Int. Conf. Comput.-Aided Design (ICCAD)*, Nov. 2012, pp. 333–340.

[38] X. H. Yuan, X. W. Wu, J. Wang, Y. P. Wu, and T. V. Ree, "Solar-driven fuel production by metal-oxide thermochemical cycles," in *Metal Oxides Energy Technologies*. Amsterdam, The Netherlands: Elsevier, 2018, pp. 321–340.

[39] B. L. Wang, J. C. Han, and Y. G. Sun, "A finite element/finite difference scheme for the non-classical heat conduction and associated thermal stresses," *Finite Elements Anal. Des.*, vol. 50, pp. 201–206, Mar. 2012.

[40] J.-L. Briaud and A. Chaouch, "Hydrate melting in soil around hot conductor," *J. Geotechnical Geoenvironmental Eng.*, vol. 123, no. 7, pp. 645–653, Jul. 1997.

[41] N. E. Bixler, "An improved time integrator for finite element analysis," *Commun. Appl. Numer. Methods*, vol. 5, no. 2, pp. 69–78, Feb. 1989.

[42] *Thermoelectric Cooler*. Accessed: Jun. 2016. [Online]. Available: https://cn.comsol.com/model/download/766871/applications.thermoelectric_cooler.pdf

[43] X. Y. Zhang, X. Dai, H.-L. Kao, B.-H. Wei, Z. Y. Cai, and Q. Xue, "Compact LTCC bandpass filter with wide stopband using discriminating coupling," *IEEE Trans. Compon., Packag., Manuf. Technol.*, vol. 4, no. 4, pp. 656–663, Apr. 2014.
[44] J.-X. Xu and X. Y. Zhang, "Single- and dual-band LTCC filtering switch with high isolation based on coupling control," *IEEE Trans. Ind. Electron.*, vol. 64, no. 4, pp. 3137–3146, Apr. 2017.
[45] Q. Q. Liu, M. Zhuang, W. Zhan, N. Liu, and Q. H. Liu, "An efficient thin layer equivalent technique of SETD method for thermo-mechanical multi-physics analysis of electronic devices," *Int. J. Heat Mass Transf.*, vol. 192, Aug. 2022, Art. no. 122816.

NA LIU (Member, IEEE) received the B.S. degree in information and computation science from Henan University, Kaifeng, China, in 2008, and the Ph.D. degree in computational mathematics from the University of Chinese Academy of Sciences, Beijing, China, in 2013. From 2013 to 2017, she was a Postdoctoral Researcher at the Institute of Electromagnetics and Acoustics, Xiamen University. Since March 2017, she is an Associate Professor with the Institute of Electromagnetics and Acoustics, Xiamen University. Her research interests include computational electromagnetics, especially the fast and efficient methods for complex media and their applications in optical waveguide problems and IC simulations.

CHENYANG WANG received the B.S. degree in microelectronics science and engineering from Anhui University, Hefei, China, in 2019. He is currently pursuing the M.S. degree in electromagnetic field and microwave technology with Xiamen University, Xiamen, China. His current research interest includes computational electromagnetics.

XI CHEN received the B.S. degree in communication engineering from the China University of Geosciences, Wuhan, China, in 2018, and the M.S. degree in electromagnetic field and microwave technology from Xiamen University, Xiamen, China. His current research interests include computational electromagnetic and the fast and efficient methods in IC simulations.

QIUYUE WU received the B.S. degree in electronic information engineering from the Hunan University of Technology, Zhuzhou, China, in 2020. She is currently pursuing the M.S. degree in electronic information with Xiamen University, Xiamen, China. Her current research interest includes computational electromagnetics.

QIQIANG LIU received the B.S. degree in optical information science and technology from the Tianjin University of Technology and Education, Tianjin, China, in 2016, and the M.S. degree in integrated circuit engineering from Ningbo University, Ningbo, China, in 2019. He is currently pursuing the Ph.D. degree with Xiamen University, Xiamen, China. His current research interests include numerical methods in heat transfer, elastic wave, electromagnetics, and multi-physical co-simulation.

MINGWEI ZHUANG (Member, IEEE) received the B.S. degree in applied physics from Shandong Jiaotong University, Jinan, China, in 2011, and the Ph.D. degree in radio physics from Xiamen University, Xiamen, China, in 2018. From 2016 to 2017, he was a Visiting Student at the Department of Electrical and Computer Engineering, Duke University, Durham, NC, USA. His research interests include numerical methods in acoustic waves, elastic wave, electromagnetic, and multiphysics.

LINLIN SHI received the B.S. degree from the Department of Mathematics, Fuyang Normal College, Fuyang, China, in 2002, and the M.S. degree in basic mathematics from East China Normal University, Shanghai, China, in 2007, and Ph.D. degree from Xiamen University, Xiamen, China, in 2017. He is currently a Senior Engineer with the Fifth Electronics Research Institute of Ministry of Industry and Information Technology, Guangzhou, China. His research interests include forward modeling with finite element and spectral element methods, inverse problems in geophysical exploration, pyrognostics health management (PHM), and machine-learning techniques.

QING HUO LIU (Fellow, IEEE) received the B.S. and M.S. degrees in physics from Xiamen University, China, and the Ph.D. degree in electrical engineering from the University of Illinois at Urbana–Champaign.

He was a Research Assistant at the Electromagnetics Laboratory, University of Illinois Urbana-Champaign, from September 1986 to December 1988, and a Postdoctoral Research Associate, from January 1989 to February 1990. He was a Research Scientist and a Program Leader with Schlumberger-Doll Research, Ridgefield, CT, USA, from 1990 to 1995. From 1996 to May 1999, he was an Associate Professor at New Mexico State University. Since June 1999, he has been with Duke University, where he is now a Professor of electrical and computer engineering. His research interests include computational electromagnetics and acoustics, inverse problems, and their application in nanophotonics, geophysics, biomedical imaging, and electronic packaging. He has published widely in his research areas.

Dr. Liu is a fellow of the Acoustical Society of America, the Electromagnetics Academy, and the Optical Society of America. He has served as an IEEE Antennas and Propagation Society Distinguished Lecturer. He received the 1996 Presidential Early Career Award for Scientists and Engineers (PECASE) from the White House, the 1996 Early Career Research Award from the Environmental Protection Agency, and the 1997 CAREER Award from the National Science Foundation. He received the 2017 Technical Achievement Award and the 2018 Computational Electromagnetics Award from the Applied Computational Electromagnetics Society, and the 2018 Harrington-Mittra Award in computational electromagnetics from IEEE Antennas and Propagation Society. In 2018, he also received the University of Illinois at Urbana-Champaign ECE Distinguished Alumni Award. He was the Founding Editor-in-Chief of the IEEE JOURNAL ON MULTISCALE AND MULTIPHYSICS COMPUTATIONAL TECHNIQUES.